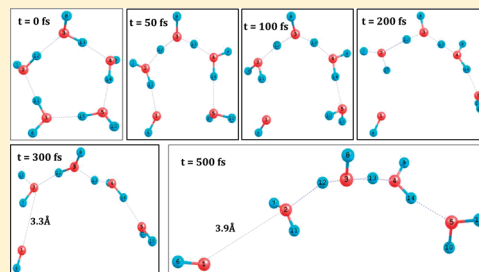


# A Density Functional Theory for Studying Ionization Processes in Water Clusters

Ester Livshits, Rebecca S. Granot, and Roi Baer\*

Fritz Haber Center for Molecular Dynamics, Chaim Weizmann Institute of Chemistry, The Hebrew University of Jerusalem, Jerusalem 91904, Israel

**ABSTRACT:** A generalized Kohn–Sham (GKS) approach to density functional theory (DFT), based on the Baer–Neuhauser–Livshits range-separated hybrid, combined with *ab initio* motivated range-parameter tuning is used to study properties of water dimer and pentamer cations. The water dimer is first used as a benchmark system to check the approach. The present brand of DFT localizes the positive charge (hole), stabilizing the proton transferred geometry in agreement with recent coupled-cluster calculations. Relative energies of various conformers of the water dimer cation compare well with previously published coupled cluster results. The GKS orbital energies are good approximations to the experimental ionization potentials of the system. Low-lying excitation energies calculated from time-dependent DFT based on the present method compare well with recently published high-level “equation of motion-coupled-cluster” calculations. The harmonic frequencies of the water dimer cation are in good agreement with experimental and wave function calculations where available. The method is applied to study the water pentamer cation. Three conformers are identified: two are Eigen type and one is a Zundel type. The structure and harmonic vibrational structure are analyzed. The ionization dynamics of a pentamer water cluster at 0 K shows a fast <50 fs transient for transferring a proton from one of the water molecules, releasing a hydroxyl radical and creating a protonated tetramer carrying the excess hole.



## I. INTRODUCTION

Absorption of ionizing radiation by aqueous systems has considerable implications for a broad variety of fields, such as chemistry of the ionosphere, waste remediation, environmental cleanup, radiation processing, nuclear reactions, and medical diagnosis and therapy.<sup>1</sup> Various processes of water ionization have been studied experimentally, finding a high abundance of protonated water clusters.<sup>2,3</sup> Molecular beam experiments confirmed this finding and determined the preferred protonated “magic number” clusters sizes.<sup>3</sup> Unprotonated cation clusters were found in Ar-seeded beams, where excess energy can be released as kinetic energy of emitted Ar atoms.<sup>4</sup>

A large number of experimental and theoretical studies have been published concerning the electronic structure and ionization dynamics of water clusters<sup>5–10</sup> as well as the vibrational properties of both protonated<sup>11</sup> and unprotonated<sup>12–15</sup> products. Additional detailed experimental results including at the attosecond and femtosecond time scales are becoming available concerning the electronic structure and ionization potentials and dynamics in water.<sup>16,17</sup>

Gaining a detailed understanding of these ionization processes has so far been hampered by the complexities involved in developing a sound theoretical approach for describing them. Impressive algorithmic developments and increased computational speed have allowed high level *ab initio* studies shedding light on the ionization dynamics in clusters of the water dimer.<sup>7–9,17</sup> However, these methods are limited to small clusters due to the steep increase in algorithmic complexity as the number of electrons

and atoms grows. What is needed is a method that can deliver useful accuracy at moderate algorithmic complexities. Such approaches are often found within the density functional theory (DFT) which for many systems delivers a favorable blend of accuracy and applicability.<sup>18</sup> The strengths and weaknesses of DFT for studying dynamical aqueous processes as well as other electronic properties are subjects of considerable theoretical interest.<sup>19,20</sup> For ionized water dimers the usual methods of DFT (i.e., local spin density approximation (LSDA)<sup>21</sup> various generalized gradients approximations,<sup>22</sup> for example, BLYP,<sup>23,24</sup> as well as hybrid methods such as B3LYP<sup>25</sup>) seem to fall flat<sup>7,20,26</sup> and require either a higher hybrid mixing coefficient<sup>27</sup> or the use of self-interaction corrections.<sup>7,28</sup> The main reason for this failure has been identified as the exorbitant electron/hole delocalization due to spurious self-repulsion was demonstrated in symmetric radical cation systems.<sup>26,29–32</sup>

In this paper, a new DFT approach, recently developed for treating symmetric radical cations,<sup>32</sup> is assessed for the water cluster ionization, using experimental and high-level *ab initio* benchmark data available for the water dimer cation. The DFT method we use can be viewed as an approximation to the “in principle exact” generalized Kohn–Sham approach to DFT which uses orbital functionals, in addition to pure density

**Special Issue:** Victoria Buch Memorial

**Received:** June 22, 2010

**Revised:** September 11, 2010

functionals.<sup>33</sup> Our orbital functional is a range-separated hybrid (RSH)<sup>34–38</sup> designed to eliminate the long-range Hartree self-repulsion. A critical element in our method is the ab initio motivated range-parameter tuning<sup>32,37,39</sup> crucial for balancing the local and long-range energetics of the system. In section II we give a more detailed account of our approach and assess its performance by comparing to previous calculations and experiments. In section III the method will be used to study the structure, IR spectrum, and ionization dynamics in water dimer and pentamer clusters. A short summary and discussion is given in section IV.

## II. METHOD AND VALIDATION

Our method is an approximation within the in-principle exact generalized Kohn–Sham (GKS) approach to DFT.<sup>33</sup> GKS differs from the Kohn–Sham (KS-DFT) method.<sup>21</sup> In the latter, a system of electrons in their ground state having a density  $n(\mathbf{r})$  is mapped onto a unique system of noninteracting electrons in their ground state, described by a single Slater determinantal wave function composed of  $N$  orbitals  $\psi_n(\mathbf{r})$   $n = 1, \dots, N$ , having the same density. The KS orbitals are the lowest energy eigenstates of the single-particle KS Hamiltonian, composed of single particle operators: kinetic energy and local KS potential. GKS maps the interacting ground state electrons onto a system of “partially interacting” electrons in the lowest energy single Slater determinantal wave function having the same density  $n(\mathbf{r})$ . This mapping and associated energy minimization process results in single particle equations for the GKS orbitals which include, in addition to a single-particle kinetic energy operator and local potentials, an explicit orbital functional.<sup>33</sup> The GKS mapping defines a “residual” exchange-correlation energy functional of the density, which can in principle close the theory but which must eventually be approximated. In our approach we use the Baer–Neuhauser–Livshits<sup>36,37</sup> (BNL) range separated hybrid (RSH). The exchange energy into long- and short-range parts,  $E_X = E_{X,LR} + E_{X,SR}$ , by dissecting the electron–electron distance as

$$\frac{1}{r_{12}} = \frac{\text{erfc}(\gamma r_{12})}{r_{12}} + \frac{\text{erf}(\gamma r_{12})}{r_{12}} \quad (2.1)$$

$\gamma$  is the range parameter, differentiating between the two ranges. The explicit GKS orbital functional is the LR part

$$E_{X,LR} = -\frac{1}{2} \iint \frac{\rho(\mathbf{r}_1, \mathbf{r}_2)^2 \text{erf}(\gamma r_{12})}{r_{12}} d^3r_1 d^3r_2 \quad (2.2)$$

where  $\rho(\mathbf{r}_1, \mathbf{r}_2) = \sum_m \psi_m(\mathbf{r}_1) \psi_m(\mathbf{r}_2)$  is the GKS density matrix. The short-range exchange energy  $E_{X,SR}$  is a pure density functional, approximated by a local density expression<sup>40</sup> is

$$E_X^{\text{LDA}, \gamma} = \int \varepsilon_X^{\text{HEG}, \gamma}(n(\mathbf{r})) n(\mathbf{r}) d^3r \quad (2.3)$$

where

$$\varepsilon_X^{\text{HEG}, \gamma} = -\frac{3k_F}{4\pi} \left( 1 - \frac{2}{3} G(\gamma/k_F) \right) \quad (2.4)$$

$k_F = (3\pi^2 n)^{1/3}$  is the Fermi wave vector and

$$G(q) = q^2 [2\sqrt{\pi} \text{erf}(q^{-1}) - q + q(q^2 - 2)(1 - e^{-q^{-2}})] \quad (2.5)$$

The remaining correlation energy in GKS/BNL is not known exactly but can be approximated as  $E_C^\gamma = E_C^{\text{LYP}} - w E_X^{\text{LDA}, \gamma}$  where the first term is the LYP correlation energy<sup>24</sup> and the second involves subtraction of a small (10%) amount of the short-range exchange energy. The BNL functional is described in greater detail in ref 37.

Two theoretical benefits are obtained by this GKS approach: (1) the long-range part of the self-interaction energy, that due to the Hartree self-repulsion, is greatly reduced, and (2) a large part of the KS derivative discontinuity<sup>41</sup> is absorbed in the orbital functional reducing the necessity for finding noncontinuous density functionals.<sup>33,39,42</sup> While most applications of the RSH approach use a “universal” range-parameter  $\gamma$ ,<sup>35,37,43</sup> we find that for good quantitative results this parameter must be adapted to each system separately. Theoretical reasons are given in ref 39, and for systems involving symmetric radical cations this was shown explicitly in ref 32. In the past we have checked in our group two relevant ways to determine the range-parameter value in a first principles manner (i.e., without reference to specific empirical data). One way is motivated by the ionization potential theorem (IPT),<sup>41,44</sup> that the negative highest occupied (HO) molecular orbital (MO) energy  $-\varepsilon_H$  is equal to the ionization potential (IP). This method gave good charge-transfer excitation energies,<sup>45</sup> ionization potentials,<sup>46</sup> and Rydberg excitations<sup>39</sup> in many systems. The second method is based on the physical principle of energy degeneracy between two charged states of the well-separated dimer  $(\text{H}_2\text{O} \cdots \text{H}_2\text{O})^+$ , namely, the energies of the localized charge state (when the hole is localized on a monomer) and the symmetric delocalized state (when the hole is symmetrically delocalized between the fragments). This latter tuning method enabled quantitative description of symmetric cations such as  $\text{H}_2^+$ ,  $\text{He}_2^+$ , and  $\text{Ne}_2^+$ .<sup>32</sup> In the present study we found that the two ab initio motivated methods for determining  $\gamma$ , the IP theorem applied to  $\text{H}_2\text{O}$  and the energy degeneracy criterion applied to  $(\text{H}_2\text{O})_2^+$ , yield almost identical values for  $\gamma$ , namely, 0.56 and 0.58  $a_0^{-1}$ , respectively. This near identity has been seen in other systems and explained elsewhere.<sup>39</sup> It is related to the fact that in RSHs the GKS energy changes almost linearly as a function of HOMO occupation number,<sup>42</sup> due to small self-repulsion.<sup>42,46</sup>

The BNL functional has been coded into widely available codes (QCHEM 3.2,<sup>52</sup> Quantum Espresso,<sup>53,54</sup> and NWCHEM<sup>55</sup>). In the present paper, all electronic structure calculations were done using the QCHEM implementation. Following ref 7 we use the 6-311++G\*\* basis set; the inclusion of diffuse functions is important for decreasing basis set superposition errors.<sup>56</sup> Below we test the degree of convergence by comparing some results to those obtained by using a larger basis set, namely, aug-cc-pVQZ (see Table 2).

**A. Assessment of Orbital Energies as IPs.** We address not only water molecules, dimers, and their cations but also products of the proton transfer reaction  $(\text{H}_2\text{O})_2^+ \rightarrow \text{H}_3\text{O}^+ + \text{OH}$ . For both OH and  $\text{H}_3\text{O}^+$  the IP theorem method yields identical values  $\gamma = 0.63 a_0^{-1}$ , somewhat different from the optimal parameters of the water molecule,  $\gamma = 0.56, 0.58 a_0^{-1}$ . Consequently, there are several different values of  $\gamma$  relevant for the system we are studying. However, these values of the range parameters do not vary by much, so selecting  $\gamma = 0.6 a_0^{-1}$  seems a reasonable compromise. Indeed, this choice makes only a small deviance from the IPT for the water molecule: with  $\gamma = 0.56 a_0^{-1}$  the IP ( $\Delta\text{SCF}$ ) and  $-\varepsilon_H$  of  $\text{H}_2\text{O}$  have the identical value of 12.7 eV while for  $\gamma = 0.6 a_0^{-1}$  the  $\Delta\text{SCF}$  IP is 12.6 eV while the HOMO

**Table 1. BNL\* Orbital Energies (eV) for (H<sub>2</sub>O)<sub>2</sub> and Associated Monomers (Using the 6-311++G\*\* Basis Set) Compared with ab Initio Results and Experiments**

orbital	BNL*		EOM-IP-CCD <sup>7</sup>	exptl
H <sub>2</sub> O	$\gamma = 0.60^a$	$\gamma = 0.56^b$		
1b2	12.8	12.7	12.3	12.62 <sup>47,48</sup>
3a1	14.7	14.7	14.6	14.64, <sup>47</sup> 14.80 <sup>48</sup>
1b1	18.7	18.6	18.8	18.60 <sup>47,48</sup>
(H <sub>2</sub> O) <sub>2</sub>	$\gamma = 0.60^a$	$\gamma = 0.56^b$		
2a''	11.9	11.9	11.4	12.10 <sup>49</sup>
8a'	13.4	13.4	12.9	13.20 <sup>49</sup>
7a'	13.9	13.9	13.7	
6a'	15.6	15.6	15.4	
5a'	18.0	17.9	18.0	
4a'	19.8	19.4	19.5	
OH	$\gamma = 0.60^a$	$\gamma = 0.63^b$		
$\pi$	13.0	13.2		13.2 <sup>50</sup>
$\sigma$	13.9	14.0		
H <sub>3</sub> O <sup>+</sup>	$\gamma = 0.60^a$	$\gamma = 0.63^b$		
a1	24.8	24.1	24.4	20.0 <sup>c</sup>
E	29.7	30.2	30.2	

<sup>a</sup> $\gamma = 0.60a_0^{-1}$  is the average for (H<sub>2</sub>O)<sub>2</sub> → (H<sub>2</sub>O)<sub>2</sub><sup>+</sup> → OH + H<sub>3</sub>O<sup>+</sup>.

<sup>b</sup> $\gamma$  determined by the IP theorem for the system. <sup>c</sup> Measured for aqueous H<sub>3</sub>O<sup>+</sup>.<sup>51</sup>

energy is 12.8 eV. These values compare well with the experimental vertical ionization potential of water 12.6 eV.<sup>57</sup> We show in Table 1 a comparison of the GKS orbital energies from the BNL calculation and the experimental and/or ab initio results for the ionization potentials of relevant systems. It is evident that the GKS orbital energies after tuning the  $\gamma$  parameter give a realistic description of the ionization levels. We should mention that this result is not particular to the present systems and has recently been demonstrated to have a broader scope of applicability.<sup>39,46</sup>

**B. Assessment of the BNL\* Energetics.** In Table 2 energy differences of various configurations (metastable as well as transition state) estimated by wave function calculations<sup>7,17</sup> and several density functional methods including BNL\*. It is seen that BNL\* results are similar to the high-level ab initio wave function methods, with discrepancies of  $\leq 2$  kcal/mol. BNL\* avoids the erroneous prediction of the generalized gradients approximation (BLYP) and hybrid (B3LYP) functionals. BLYP predicts that the hemibonded (HB) configuration [(H<sub>2</sub>O)⋯(H<sub>2</sub>O)]<sup>+</sup> of the (H<sub>2</sub>O)<sub>2</sub><sup>+</sup> cation is more stable than the proton transferred (PT) configuration (H<sub>3</sub>O<sup>+</sup>⋯OH), in contrast to a wealth of post-HF ab initio calculations<sup>7,17,56,58</sup> and recent experiments.<sup>12,13</sup> BLYP, as well as other local KS approximations, destabilizes the PT complex where the positive hole is localized (on the H<sub>3</sub>O<sup>+</sup> fragment), while it stabilizes the HB complex for which charge is delocalized between the two monomers.<sup>6</sup> This can be attributed to the spurious self-repulsion in these approximations.<sup>29,32,56</sup> Hybrid GKS functionals, such as B3LYP, partially correct for the long-range self-repulsion, although they still exhibit a significant amount of overstabilization of the charge delocalized state in symmetric radical cations.<sup>30</sup> BNL\*, being a range separated hybrid, does not suffer from long-range self-repulsion; furthermore, its range parameter is tuned to balance the energies of the localized and delocalized charge states and it is thus able to deliver a good overall description of the relative energies involved. This latter issue is explained in more detail in refs 32 and 39. BNL\* predicts almost zero energy difference for the reaction

(H<sub>2</sub>O)<sub>2</sub><sup>+</sup>(N) → OH + H<sub>2</sub>O<sup>+</sup> (the symbol (N) is the stable configuration of the neutral water dimer). This is close to the ab initio result, predicting that the reaction is slightly exothermic (by less than 1 kcal/mol). Using a new saddle location method<sup>59</sup> we located the transition state and estimated the energy barrier for the isomerization reaction from the HB to the PT configuration. The barrier found by BNL\* is higher by 2 kcal/mol than the CCSD(T) prediction.<sup>17</sup> B3LYP underestimates the barrier by ~50%.

The HF method, which was used in a previous study of water dimer ionization,<sup>15</sup> does considerably better than the KS-DFT methods. However, the tendency of HF to overstabilize localized charge states relative to delocalized states overestimates the difference in energy between that of the HB configuration energy relative to the PT one. HF also predicts relatively high exothermicity of (H<sub>2</sub>O)<sub>2</sub><sup>+</sup>(N) → OH + H<sub>2</sub>O<sup>+</sup> (by 3 kcal/mol as opposed to 1 kcal/mol of CCSD(T)<sup>17</sup>). While this deviance of HF is small, it is an important one since the probability of hydroxyl radical release due to ionization is critically dependent on this energy. There is no clear experimental indication as to the energetics of hydroxyl radical release from water dimers upon ionization.

**C. Assessment of Electronic Excitations.** To further test GKS/BNL\* as an electronic structure method for the water dimer cation, we benchmarked the electronic excitations at C<sub>s</sub> proton-transferred geometry. In Table 3 we compare predictions of different methods. All excitations considered here involve transfer of electron to the half-filled orbital. The excitations can be classified as transition *within* the OH fragment and electron transfer transitions *from* H<sub>3</sub>O<sup>+</sup> to OH. The first excitation involves very low frequencies as it describes two internal transitions within the OH radical, between the filled 1 $\pi$  or 2 $\sigma$  orbitals to the half-filled 2 $\pi$  HOMO. When compared to equation of motion estimates of excitation energies<sup>7</sup> (Table 3) these two local excitations are reasonably described by the TDDFT methods, although the 2 $\sigma$  → 2 $\pi$  transition is lower by 0.5 eV in the BNL\*. However, when the nonlocal charge-transfer excitations are considered, B3LYP considerably underestimates the excitation energies when compared with the EOM results (by 2.5–3 eV) while BNL\* excitations are 0.7 eV higher than the EOM-IP results but only 0.3 eV higher than the EOM-EE result. Regarding the oscillator strengths, there is considerable misfit in this quantity between the EOM and the BNL\* (in two cases out of three). In charge transfer excitations oscillator strengths are sensitive to the overlap between exponential tails of the excited and ground state wave functions.

Summarizing this section, we described the BNL\* functional, the method of tuning its range-parameter, and presented several tests, showing it gives a good account of the cation water dimer electronic structure. In the next sections we apply our BNL\* method to the ionization of dimer and pentamer clusters.

### III. RESULTS

In this section we apply the BNL\* functional to study the water dimer and pentamer cation IR spectra and the associated ionization dynamics.

**A. Structure of the Water Dimer Cation.** The structure of the water dimer cation, predicted by BNL\* shown in the top part of Figure 1 is that of a Zundel type, where a hydrogen is “shared” by a hydroxyl (OH) radical and a water (H<sub>2</sub>O) molecule. The OH bond lengths in the H<sub>2</sub>O molecule and in the hydroxyl radical are almost identical, equal on the average to 0.989 Å. This should be



**Table 2.** Energy Differences (kcal/mol; No Vibrational Energy Corrections) Computed by BNL (0.6) with 6-311++G\*\* Basis Compared to Results of Various Methods<sup>a</sup>

A(config)	B(config)	E(A) – E(B) (kcal/mol)								
		DZV		6-311++G**					(aug)cc-pVQZ	
		BLYP	B3LYP	HF	EOM-IP-CCSD <sup>7</sup>	EOM-IP-CC(2,3) <sup>7</sup>	CCSD(T) <sup>7</sup>	BNL* (0.6)	CCSD(T) <sup>17</sup>	BNL*(0.6)
(H <sub>2</sub> O) <sub>2</sub> <sup>+</sup> (N)	OH + H <sub>2</sub> O <sup>+</sup>	–18.1	–7.7	3.8				–0	1.0	+0
(H <sub>2</sub> O) <sub>2</sub> <sup>+</sup> (PT)	(H <sub>2</sub> O) <sub>2</sub> <sup>+</sup> (N)	–6.5	–16.5	–23.7	–20.0	–21.8	–21.6	–23.6	–23.3	–25.1
(H <sub>2</sub> O) <sub>2</sub> <sup>+</sup> (HB)	(H <sub>2</sub> O) <sub>2</sub> <sup>+</sup> (PT)	–9.3	–1.8	27.1	5.3	7.4	8.2	9.7	7.1	9.5
(H <sub>2</sub> O) <sub>2</sub> <sup>+</sup> (PT)	OH + H <sub>2</sub> O <sup>+</sup>	–24.6	–24.2	–18.9				–23.6	–22.3	–25.1
(H <sub>2</sub> O) <sub>2</sub> <sup>+</sup> (TS)	(H <sub>2</sub> O) <sub>2</sub> <sup>+</sup> (PT)		7.8					17.2	15.1	17.5

<sup>a</sup> BNL results change by less than 2% when compared to the aug-cc-pVQZ basis. Nuclear geometries of (H<sub>2</sub>O)<sub>2</sub><sup>+</sup>: (N) = the neutral configuration of (H<sub>2</sub>O)<sub>2</sub>; (PT) = stable proton transferred configuration of (H<sub>2</sub>O)<sub>2</sub> (structure 1 of ref 17); (HB) = hemibonded metastable configuration of (H<sub>2</sub>O)<sub>2</sub><sup>+</sup> (structure 7 in ref 17); (TS) is the saddle configuration for the HB → PT transition (structure 10 of ref 17).

**Table 3.** Vertical Excitation Energies (eV) and Oscillator Strengths ( $\times 10^{-4}$ ) of in (H<sub>2</sub>O)<sub>2</sub><sup>+</sup> at Proton-Transferred Geometry: Comparison between TDDFT and EOM CCSD Methods at the 6-311++G\*\* Basis Set Level<sup>a</sup>

orbital	EOM-IP-CCSD <sup>7</sup>		EOM-EE-CCSD <sup>7</sup>		B3LYP		BNL* ( $\phi = 0.6$ )	
	$h\nu$	$f$	$h\nu$	$f$	$h\nu$	$f$	$h\nu$	$f$
OH <sub>1<math>\pi</math></sub>	0.5	0	0.5	0	0.7	0	0.2	0
OH <sub>2<math>\sigma</math></sub>	4.5	15	4.5	14	4.4	14	4.0	15
(H <sub>3</sub> O <sup>+</sup> ) <sub>H</sub>	8.4	29	8.9	21	5.7	2	9.2	0
(H <sub>3</sub> O <sup>+</sup> ) <sub>H-1</sub>	13.1	6			10.5	1	13.7	4
(H <sub>3</sub> O <sup>+</sup> ) <sub>H-2</sub>	14.3	8			11.0	20	15.0	50

<sup>a</sup> All excitations are to the half-filled HOMO which is the 2 $\pi$  orbital on OH.

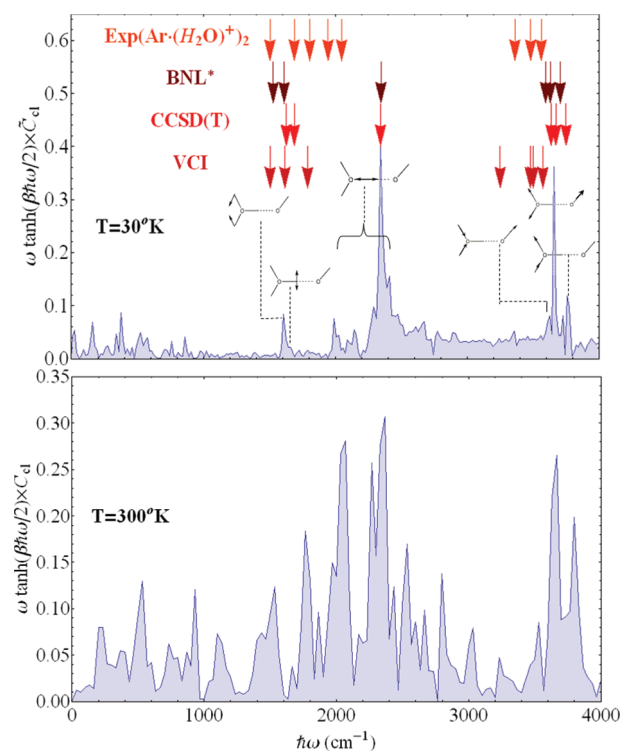
compared to the CCSD(T) results of 0.995 Å (for the cc-pVTZ<sup>27</sup>) and 0.970 Å (for the cc-pVQZ basis set<sup>17</sup>). The transferred hydrogen is closer to the hydronium oxygen, at a distance of 1.068 Å (compare to 1.048 Å in CCSD(T)<sup>17</sup>). Its distance from the oxygen of the hydroxyl radical is 1.464 Å (compare to 1.462 Å in CCSD(T)<sup>17</sup>). The corresponding O–H–O angle of these three atoms is 171.6° (compare to 173.4° in CCSD(T)<sup>17</sup>). The H–O–H angle involving the hydroxyl radical and the transferred hydrogen, 129.95° in BNL\*, is  $\sim 8^\circ$  larger than the corresponding value in CCSD(T);<sup>17</sup> this forms the largest difference in the structure predicted by the two theories.

According to the Mulliken charge analysis, all hydrogen atoms in the dimer cation seem to carry a similar charge of about +0.4, the hydronium oxygen carries the charge –0.4 while the hydroxyl oxygen carries a smaller negative charge of –0.2. Viewing the dimer as a hydronium bound to a hydroxyl radical, we can say that the hole is shared between the two entities: 80% of the hole is located on hydronium and 20% on hydroxyl. Below we show that a similar charge allocation is seen also in the two Eigen type pentamer water cations.

**B. IR Spectra of Water Dimer Cation.** The calculated IR absorption spectrum involves an estimation of the thermal average of the dipole–dipole correlation functions

$$C(t) = \frac{1}{3} \sum_i \langle \hat{M}_i \hat{M}_i(t) \rangle \quad (3.1)$$

where  $\hat{M}_i$  is the dipole moment in direction  $i$ ,  $i = x, y, z$  of (H<sub>2</sub>O)<sub>2</sub><sup>+</sup>. (comment: even though the dipole of a charged

**Figure 1.** IR absorption spectrum of the water dimer. The spectrum obtained from classical AIMD at 30 K (top) and 300 K (bottom) is shown together with arrows indicating experimental,<sup>12</sup> BNL\*/harmonic, CCSD(T)/harmonic,<sup>17</sup> and EOM-IP-CC/VCI frequencies.<sup>9</sup> BNL\* harmonic normal mode assignments are indicated as well.

system is arbitrarily dependent on the position of the coordinate origin, the AC part of the spectrum is well-defined since  $\langle \hat{M}_i(t) \rangle$  is time-independent). Thermal averaging is attained by sampling an Andersen thermostat<sup>60</sup> stochastic dynamics trajectory of (H<sub>2</sub>O)<sub>2</sub><sup>+</sup> at temperature  $T$  (30 and 300 K). The first 0.5 ps of the trajectory were discarded and subsequently  $M = 10$  configurations at intervals of 100 fs were used to produce, via a microcanonical AIMD simulation dipole moment signals  $M_i(t)$  ( $i = x, y, z$ ) as a function of time  $t$  (at 10 au intervals). The trajectory average

$$\overline{C_d}(t) = \frac{1}{3} \sum_{i=x,y,z} \overline{M_i M_i(t)} \quad (3.2)$$

was used to estimate the IR spectrum using the formula<sup>61</sup>  
 $n(\omega)\alpha(\omega) \propto \omega \tanh(\beta\hbar\omega/2)\tilde{C}_d(\omega)$ , where  $\tilde{C}_d(\omega) = \int_{-\infty}^{\infty} \tilde{C}_d(t)e^{-i\omega t} dt$ . The spectrum obtained in this way is shown in Figure 1 for 30 and 300 K. The peaks are compared to calculated harmonic frequencies based on CCSD(T)<sup>17</sup> and to anharmonic variational CI frequencies based on EOM-IP-CCSD PESs<sup>9</sup> and to experimental vibrational predissociation spectra for  $\text{Ar}\cdot(\text{H}_2\text{O})_2^+$ .<sup>12</sup> The 30 K peaks correspond closely to the shown harmonic BNL lines. The latter are in reasonable agreement with the CCSD(T) harmonic spectrum. The water bend frequencies of the present calculations are red-shifted relative to the CCSD(T) harmonic frequencies by 50–80  $\text{cm}^{-1}$  but are in closer agreement with experiment and EOM-IP-CC/VCI results.

The high end of the spectrum dominated by the OH vibrations shows similar trends: BNL\* harmonic frequencies are red-shifted by 50–100  $\text{cm}^{-1}$  relative to the CCSD(T) harmonic results but agree more closely to experiment. On comparison to the EOM-IP-CC/VCI spectrum (which includes quantum anharmonic effects), the harmonic spectra are similar with one noticeable deviation: the harmonic  $\nu_{\text{spl}}$  peak at 2370  $\text{cm}^{-1}$  is considerably red-shifted (by about 400  $\text{cm}^{-1}$ ) in the anharmonic spectrum. This was attributed to anharmonic mixing of the hydrogen vibration with that of O–O vibrational mode.<sup>9,17</sup> As the lines involve hydrogen vibration, our classical calculation at 30 K does not significantly sample the anharmonic structure of the potential. The 300 K spectrum on the other hand does exhibit many anharmonic effects, and a considerably larger number of lines are seen. The lines at 2370  $\text{cm}^{-1}$  are shifted to the red by about 100  $\text{cm}^{-1}$ , and a considerable vibrational activity is seen at 1550  $\text{cm}^{-1}$  in accordance with the experimental lines and VCI spectra.

**C. Ionization Dynamics of the Water Dimer.** We now apply the method for studying molecular dynamics (MD) of a small ionized water cluster, in a special ionized water dimer cluster and water pentamer cluster. The calculations were done using ab initio (Born–Oppenheimer) molecular dynamics (AIMD) implemented in Q-Chem 3.2<sup>52</sup> software. The dynamics corresponds to a Franck–Condon approximation, where the ionization is immediate so the initial nuclear configuration is that of stable water dimer, but the electronic wave function is that of the ground state cation.

The two water molecules in the neutral dimer are bound by a hydrogen bond (HB). We find that upon ionization the initial hole forms on the HB donor (HBD), a fact seen also in HF and EOM-CC calculations.<sup>7,15</sup> Formation of a hole on the HB acceptor (HBA) is higher in energy by about 1.5 eV. In Figure 2 (top panel) we plot the distance of the transferred proton from the two oxygen nuclei. Initially the proton is transferred from Od to Oa within about 18 fs. At the same time the heavier O nuclei start moving toward each other, albeit on a slower time scale, reaching a minimal distance of 2.4 Å at  $t = 35$  fs. The proton bounces back and forth twice between the two O nuclei during the process. Finally, the latter start receding at  $t = 45$  fs. When the O atoms move to a distance larger than 2.6 Å, the proton localizes on Oa. However, the Oa–Od vibration brings these atoms to closer proximity again at  $t = 140$  fs. Once close, the proton again delocalizes and oscillates between them. This happens at  $t = 250$  fs. The trajectory stops at 320 fs because of failure of SCF to converge (the proximity of the excited state, situated on the OH radical, plagues the SCF convergence throughout the calculation). The dynamics seen in the present calculation is different from that described using a Hartree–Fock (HF) electronic structure.<sup>15</sup> In HF, the initial proton transfer is slower, taking 30 fs, then the proton oscillates 3 times between Od and Oa and at 50 fs localizes on Od for 60 fs.

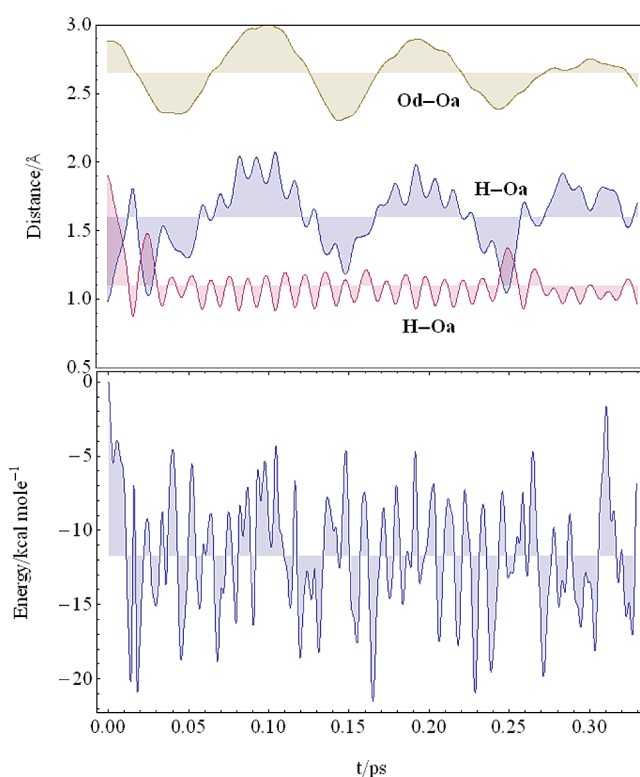


**Figure 2.** AIMD trajectory for the photoionization of the water dimer at 0 K: (top) selected atom–atom distances vs time  $t$  since photoionization of the water dimer. Od (Oa) is the donor (acceptor) oxygen while H is the transferred proton. (bottom) Potential energy changes vs  $t$ .

Only then does the proton move to Oa and stays localized on it for at least 150 fs. Furthermore, the maximal O–O distance in the HF calculation reaches 3.25 Å while in the present calculation it is only 3.0 Å. This larger amplitude is due to the weaker hydroxyl radical–protonated water cation bond predicted by the HF calculation. Indeed dissociation of the hydroxyl radical leaving hydronium behind is energetically possible according to Hartree–Fock (exothermic by 3.8 kcal/mol, see Table 2) but forbidden in the present DFT calculation (exothermicity is 0 kcal/mol, see Table 2). The present full dimensional dynamics can be compared with the reduced dimension wave packet quantum dynamics in ref 9 where only the O–O and H–Oa are considered. The similarity in the calculation is that a similar trend is observed, where the O–O distance is initially reduced while the O–H distance vibrates several times. However, the quantum dynamics is ended after 50 fs and thus cannot see the O–O receding and vibrating. This brief time is also not sufficient to determine just how close the two oxygen atoms approach each other. In our calculation the closest distance is 2.35 Å while the quantum calculation is stopped when the O–O distance is significantly larger. Obviously, in our calculation the O–O vibration is significantly faster.

The changes in the potential energy (=negative changes in kinetic energy) in the dimer as a function of time since photoionization are shown in Figure 2 (bottom). The average energy change is 12 kcal/mol with strong and rapid oscillations of amplitude between −9 and +7 kcal/mol. In the Hartree–Fock calculation the average potential energy is similar but the oscillations have larger amplitude (−11 to +11 kcal/mol) and the rate of oscillations is different.

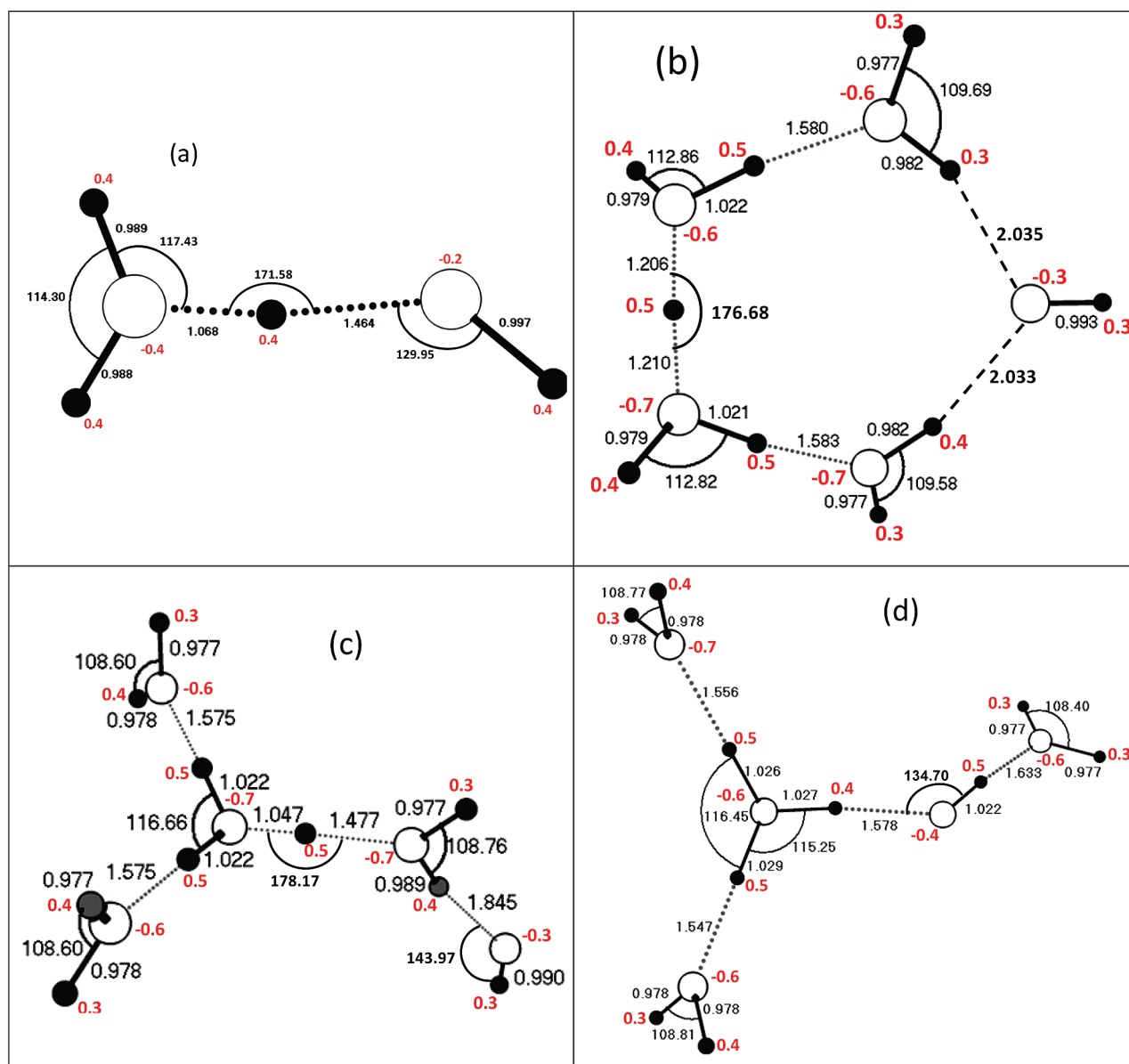


**Figure 3.** Basic structures, distances between neighboring atoms (Å), and angles in black and Mulliken charges in red, of the water dimer cation (a) and water pentamer cations (b–d) predicted by the BNL\*/6-311++G\*\* theory.

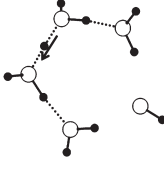
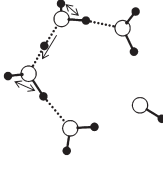
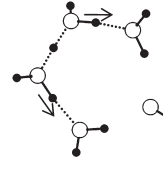
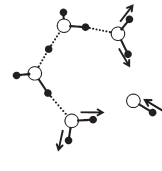
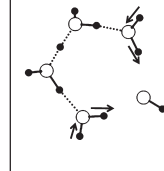
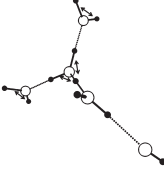
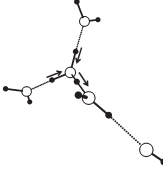
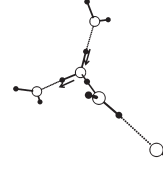
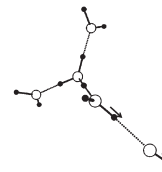
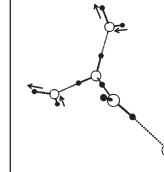
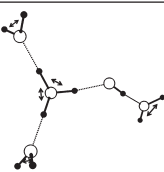
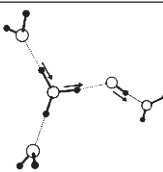
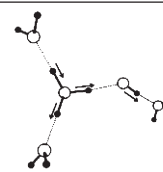
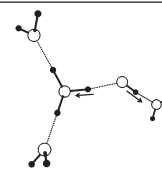
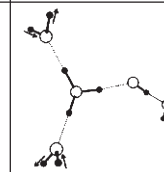
**D. Structures of Water Pentamer Cation.** We now consider the water pentamer cation and ionization process. The three conformers of the water pentamer cation are shown in Figure 3b–d. The first structure considered (Figure 3b) involves a ringlike conformation, where the hydroxyl radical OH is bound from both sides to a bent–linear protonated tetramer ( $\text{H}^+\text{O}_4\text{H}_8$ ). The bent tetramer involves a proton in a Zundel type  $\text{O}\cdots\text{H}\cdots\text{O}$  bond connecting two water dimers. This Zundel conformer is 0.05 eV higher in energy than the lowest Eigen conformer considered next. The structure of this conformer is similar to the lowest energy geometry of water pentamer (see the  $t = 0$  panel of Figure 5) and thus relevant for low-temperature IR spectra taken from pentamer cations formed by photoionization of the pentamer in an Ar seeded beam. The positive charge of the tetramer is located on the Zundel proton and the two water molecules connected to it.

In the lowest energy structure is an Eigen structure (Figure 3c) where the central hydronium ( $\text{H}_3\text{O}^+$ ) binds three water

molecules and the hydroxyl radical is attached to one of the end water molecules. Eighty percent of the cation charge is localized on this hydronium. A second Eigen structure, almost identical in energy to the first (higher by 0.02 eV) is shown in Figure 3d where it is the OH radical which is bonded to the hydronium and the third water molecule binds to the hydroxyl. The closeness of energies between these two isomers indicates that they can coexist in an ensemble at room temperature. As in the first Eigen conformer, here too 80% of the charge is located on the hydronium, with the hydroxyl carrying the rest of the charge.

**E. IR Spectra of Water Pentamer Cations.** Calculated harmonic frequencies related to hydrogen vibrations of the water pentamer cation conformers are shown in Table 4. Only strong absorption lines are shown (for a complete list of harmonic data, including the frequencies and normal modes. The Zundel structure is unique in that the shared proton has a low vibrational

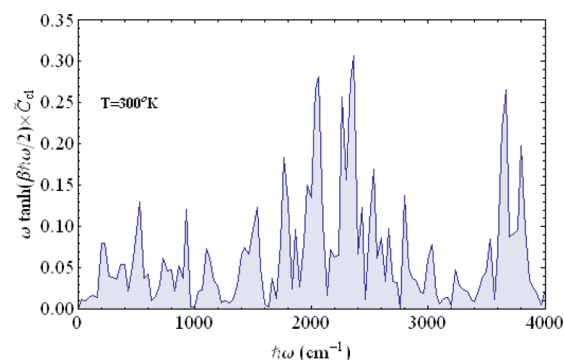
**Table 4.** Calculated Harmonic Frequencies ( $\text{cm}^{-1}$ ) and Vibrational Modes Related to Hydrogen Motion in the Water Pentamer Conformers

Zundel	 880	 1710	 3060	 3740	 3860
Eigen 1	 1580	 2610	 3000	 3610	 3880
Eigen 2	 1580	 2870	 2890	 3170	 3880

frequency (at  $880\text{ cm}^{-1}$ ). The HOH bending modes have frequencies in the range  $1600\text{--}1750\text{ cm}^{-1}$ . The Zundel structure does not exhibit strong vibrational lines in the frequency region  $1750\text{--}3000\text{ cm}^{-1}$ , and in the region  $3000\text{--}4000\text{ cm}^{-1}$  it displays strong absorption lines due to hydrogen stretching vibrational modes. Both Eigen structures exhibit significant activity also in the region  $2500\text{--}3100\text{ cm}^{-1}$ ; these vibrations are due to hydrogen vibrational motion in the hydronium. The OH stretching models of the outer water molecules and the OH radical form the highest features in the spectrum,  $3600\text{--}3900\text{ cm}^{-1}$ .

The calculated anharmonic IR spectra at 300 K of the pentamer cation was produced using classical molecular dynamics in basically the same way as described for the dimer cation. We used 9 1ps AIMD trajectories for averaging the correlation function, taking their initial configuration and velocities from a 300 K Andersen thermostat trajectory.<sup>60</sup> The spectrum of the average correlation functions corrected for quantum statistics as discussed above are shown in Figure 4. The spectrum reveals a great wealth of vibrational lines, which are due to a combination of anharmonic effects and the Boltzmann statistical coexistence of the Zundel (10%), Eigen1 (60%), and Eigen2 (30%) clusters. The low-frequency bands (at around  $200\text{--}400\text{ cm}^{-1}$ ) involve significant O–O vibrations in the normal modes while most of the stronger bands at higher frequencies can be related to the above values of harmonic frequencies for the various cluster configurations (see Table 4). The strong peaks at  $2000\text{ cm}^{-1}$  where there are no harmonic frequencies, are a result of the strong anharmonicities in the underlying potential surface.

**F. Ionization Dynamics of the Water Pentamer.** The ionization dynamics is studied using the Franck–Condon approximation, assuming that the initial geometry of the cluster is that of the ground state pentamer. Several snapshots at the

**Figure 4.** The anharmonic spectrum of the pentamer cation at 300 K, computed from the windowed Fourier transform of the dipole–dipole correlation function averaged AIMD trajectories.

dynamics are shown in Figure 5. Within a few dozen femtoseconds O1 transfers a proton (H11) to O2 and the hydrogen bond with O5 is broken. This releases the hydroxyl radical O1–H6 from the cluster. The latter forms an elongated protonated tetramer, replacing the original ringlike structure. Subsequently, a series of concerted proton transfer processes occur, with H12 moving from O2 to O3 and H13 from O3 toward O4. In Figure 6 we show the total charge on each water molecule in the tetramer (depicted by its oxygen atom) as a function of time. It is seen, that initially the charge oscillates between O1 and O2. As mentioned above, after about 50 fs the hole irreversibly leaves O1 (releasing a hydroxyl radical) and a vibrationally excited protonated tetramer is left. Interestingly, this is a similar time scale that characterizes the proton transfer in the dimer cation. We see that the hole is not immobile but spends most of the time oscillating between O3 and



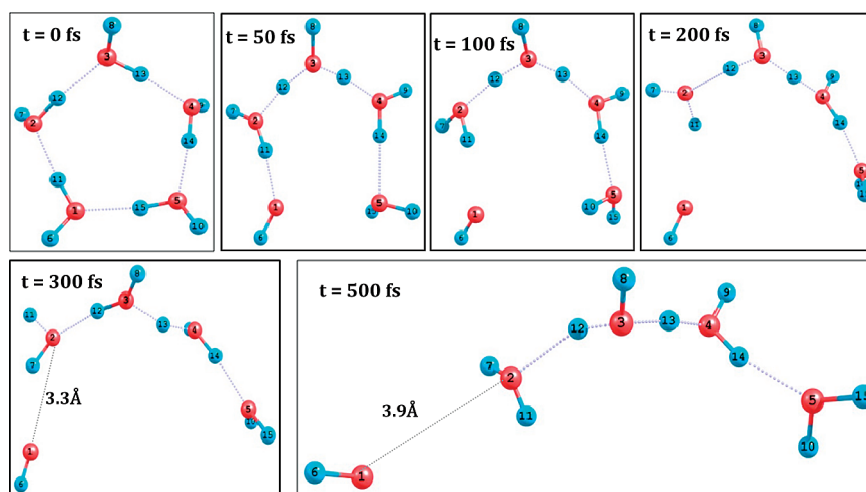


**Figure 5.** Snapshots of the photoionization dynamics of the water pentamer (starting from the neutral pentamer ground state).

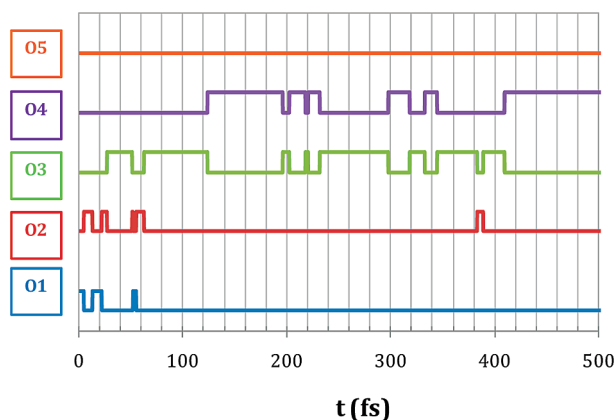


**Figure 6.** The quantized charge on each water molecule (numbered by its oxygen atom, see Figure 5) vs time  $t$  after photoionization. At  $t = 0$ , molecule O1 is positively charged while all others are neutral.

O4, with occasional visits to O2. One can time average the trajectory and reveal the “average” structure of the complex. We find it is that of a Zundel-type protonated cluster with a middle proton connecting two water dimers. This result correlates with experimental and computational studies of protonated water clusters  $\text{H}^+(\text{H}_2\text{O})_n$  ( $n = 2-5$  (ref 62) and  $n = 27$  (ref 63)).

#### IV. SUMMARY AND DISCUSSION

The failures of local and semilocal density functionals for studying the ionized symmetric cation radicals, such as  $\text{H}_2^+$ ,  $\text{He}_2^+$ ,  $\text{Ne}_2^+$ , etc., and the water dimer cation  $(\text{H}_2\text{O})_2^+$  has motivated the development of a new approach, which is the subject of this paper. Our method, BNL\*, is based on the generalized Kohn–Sham approach to DFT, employing a RSH orbital functional with a tuned range parameter. The tuning is performed in first principles ways, discussed in several former publications.<sup>32,36,37,39,45,46,54,64</sup> The first part of the paper assessed the quality of the method for the water–cation dimer and related systems, by comparing to high level wave function methods and experiments, where possible. We found that our “tuned” BNL\* functional is appropriate for describing the electronic structure and the underlying potential surface, including internal barriers, ionization energies, excited state energies, and vibrational spectrum of the water dimer cation.

Using our method we studied the vibrational and ionization dynamics of the water dimer and pentamer cations. In the pentamer, we found that the time scale for the initial proton transfer (from O1 to O2) is performed very fast, within about 10–20 fs; O1 is the oxygen of the hydroxyl. The proton subsequently moves (within 20–30 fs) to O3 and then spends most of its time on the O3–O4 dimer (see Figure 6). Future studies should address yet larger clusters, striving to reach near aqueous conditions as done, for example, in ref 10 using the Hartree–Fock approach.

The present work shows that by addressing the issue of self-repulsion and using the tuning procedure it is possible to improve considerably the range of applications of DFT for systems such as the present, where charge localization is a dominant feature. Using the suggested approach, larger water systems may be accessible for study using DFT approaches. The value of the range parameter found most suitable for the problem studied here is  $0.6 a_0^{-1}$  corresponding to a separation distance of 0.9 Å. This is extremely short, well below the bond length between first row heavy atoms (C, N, O). The results for the properties considered, geometry, ionization, and excitation and binding energies of the water molecule and water dimer cation ion, are however impressive. However, switching to full exact exchange at such short-range could have some drawbacks, especially the disturbance of the delicate cancellation of long-range exchange and long-range (static) correlation which is part of the success of local/semilocal functionals. This issue of the complementarity between static correlation and delocalization errors is currently at the forefront of current research in density functionals.<sup>38,65</sup>

#### ACKNOWLEDGMENT

We gratefully thank Professor Anna Krylov for introducing us to this interesting system and for her useful comments on the manuscript. This work was supported by the US–Israel Binational Science Foundation.

#### REFERENCES

- (1) Garrett, B. C.; Dixon, D. A.; Camaioni, D. M.; Chipman, D. M.; Johnson, M. A.; Jonah, C. D. *Chem. Rev.* **2005**, *105*, 355.
- (2) Lin, S.-S. *Rev. Sci. Instrum.* **1973**, *44*, S16. Searcy, J. Q.; Fenn, J. B. *J. Chem. Phys.* **1974**, *61*, 5282. Ng, C. Y.; Trevor, D. J.; Tiedemann, P. W.;



Ceyer, S. T.; Kronebusch, P. L.; Mahan, B. H. *J. Chem. Phys.* **1977**, *67*, 4235. Lancaster, G. M.; Honda, F.; Fukuda, Y.; Rabalais, J. W. *J. Am. Chem. Soc.* **1979**, *101*, 1951.

(3) Nagashima, U.; Shinohara, H.; Nishi, N.; Tanaka, H. *J. Chem. Phys.* **1986**, *84*, 209.

(4) Shinohara, H.; Nishi, N.; Washida, N. *J. Chem. Phys.* **1986**, *84*, 5561.

(5) Lathan, W. A.; Curtiss, L. A.; Hehre, W. J.; Lisle, J. B.; Pople, J. A. *Molecular Orbital Structures for Small Organic Molecules and Cations. In Progress in Physical Organic Chemistry*; Cohen, S. G., Streitwieser, A., Taft, R. W., Eds.; Wiley: Hoboken, NJ, 2007; p 175. Tomoda, S.; Kimura, K. *Chem. Phys. Lett.* **1983**, *102*, 560. Tomoda, S.; Kimura, K. *Chem. Phys. Lett.* **1983**, *82*, 215. Tomoda, S.; Kimura, K. *Chem. Phys. Lett.* **1984**, *111*, 434. Lathan, W. A.; Curtiss, L. A.; Hehre, W. J.; Lisle, J. B.; Pople, J. A. *Molecular Orbital Structures for Small Organic Molecules and Cations. In Progress in Physical Organic Chemistry*; Cohen, S. G., Streitwieser, A., Taft, R. W., Eds.; Wiley: Hoboken, NJ, 1974; Vol. 11; p 175. Wroblewski, T.; Ziemczonek, L.; Karwasz, G. P. *Czech. J. Phys.* **2004**, *54*, C747. Adriaanse, C.; Sulpizi, M.; VandeVondele, J.; Sprik, M. *J. Am. Chem. Soc.* **2009**, *131*, 6046. Ginovska, B.; Camaioni, D. M.; Dupuis, M. *J. Chem. Phys.* **2007**, *127*.

(6) Barnett, R. N.; Landman, U. *J. Phys. Chem. A* **1997**, *101*, 164.

(7) Pieniazek, P. A.; VandeVondele, J.; Jungwirth, P.; Krylov, A. I.; Bradforth, S. E. *J. Phys. Chem. A* **2008**, *112*, 6159.

(8) Pieniazek, P. A.; Sundstrom, E. J.; Bradforth, S. E.; Krylov, A. I. *J. Phys. Chem. A* **2009**, *113*, 4423.

(9) Kamarchik, E.; Kostko, O.; Bowman, J. M.; Ahmed, M.; Krylov, A. I. *J. Chem. Phys.* **2010**, *132*, 194311.

(10) Furuhashi, A.; Dupuis, M.; Hirao, K. *J. Chem. Phys.* **2006**, *124*, 164310.

(11) Sato, K.; Tomoda, S.; Kimura, K.; Iwata, S. *Chem. Phys. Lett.* **1983**, *95*, 579. Yeh, L. I.; Okumura, M.; Myers, J. D.; Price, J. M.; Lee, Y. T. *J. Chem. Phys.* **1989**, *91*, 7319. Kaledin, M.; Kaledin, A. L.; Bowman, J. M.; Ding, J.; Jordan, K. D. *J. Phys. Chem. A* **2009**, *113*, 7671. Asmis, K. R.; Pivonka, N. L.; Santambrogio, G.; Brummer, M.; Kaposta, C.; Neumark, D. M. *Science* **2003**, *299*, 1375. Fridgen, T. D.; McMahon, T. B.; MacAleese, L.; Lemaire, J.; Maitre, P. *J. Phys. Chem. A* **2004**, *108*, 9008. Hammer, N. I.; Diken, E. G.; Roscioli, J. R.; Johnson, M. A.; Myshakin, E. M.; Jordan, K. D. *J. Chem. Phys.* **2005**, *122*, Cheng, H. P.; Barnett, R. N.; Landman, U. *Chem. Phys. Lett.* **1995**, *237*, 161.

(12) Gardenier, G. H.; Johnson, M. A.; McCoy, A. B. *J. Phys. Chem. A* **2009**, *113*, 4772.

(13) Angel, L.; Stace, A. *Chem. Phys. Lett.* **2001**, *345*, 277.

(14) Angel, L.; Stace, A. J. *J. Phys. Chem. A* **1999**, *103*, 2999.

(15) Tachikawa, H. *J. Phys. Chem. A* **2002**, *106*, 6915.

(16) Sander, M. U.; Luther, K.; Troe, J. *J. Phys. Chem.* **1993**, *97*, 11489. Crowell, R. A.; Bartels, D. M. *J. Phys. Chem.* **1996**, *100*, 17940. Bartels, D. M.; Crowell, R. A. *J. Phys. Chem. A* **2000**, *104*, 3349. Winter, B.; Weber, R.; Widdra, W.; Dittmar, M.; Faubel, M.; Hertel, I. V. *J. Phys. Chem. A* **2004**, *108*, 2625. Elles, C. G.; Jailaubekov, A. E.; Crowell, R. A.; Bradforth, S. E. *J. Chem. Phys.* **2006**, *125*, No. 044515. Nordlund, D.; Ogasawara, H.; Bluhm, H.; Takahashi, O.; Odelius, M.; Nagasono, M. *Phys. Rev. Lett.* **2007**, *99*, 217406. Elles, C. G.; Rivera, C. A.; Zhang, Y.; Pieniazek, P. A.; Bradforth, S. E. *J. Chem. Phys.* **2009**, *130*.

(17) Cheng, Q.; Evangelista, F. A.; Simmonett, A. C.; Yamaguchi, Y.; Schaefer, H. F. *J. Phys. Chem. A* **2009**, *113*, 13779.

(18) Parr, R. G.; Yang, W. *Density Functional Theory of Atoms and Molecules*; Oxford University Press: Oxford, 1989. Kohn, W.; Becke, A. D.; Parr, R. G. *J. Phys. Chem.* **1996**, *100*, 12974. Capelle, K. *Braz. J. Phys.* **2006**, *36*, 1318. Gidopoulos, N. I.; Wilson, S. *The fundamentals of electron density, density matrix, and density functional theory in atoms, molecules, and the solid state*; Kluwer Academic Publishers: Dordrecht and Boston, 2003. Fiolhais, C.; Nogueira, F.; Marques, M. A. *A primer in density functional theory*; Springer: Berlin and New York, 2003. Geerlings, P.; De Proft, F.; Langenaeker, W. *Chem Rev* **2003**, *103*, 1793. Siegbahn, P. E. M.; Blomberg, M. R. A. *Annu. Rev. Phys. Chem.* **1999**, *50*, 221.

(19) Mattsson, A. E.; Mattsson, T. R. *J. Chem. Theory Comput.* **2009**, *9*, 887. Santra, B.; Michaelides, A.; Scheffler, M. *J. Chem. Phys.* **2009**, *131*, 124509. Hammond, J. R.; Govind, N.; Kowalski, K.; Autschbach, J.;

Xantheas, S. S. *J. Chem. Phys.* **2009**, *131*, 214103. Kuhne, T. D.; Krack, M.; Parrinello, M. *J. Chem. Theory Comput.* **2009**, *9*, 235. Lin, I. C.; Seitsonen, A. P.; Coutinho-Neto, M. C. D.; Tavernelli, I.; Rothlisberger, U. *J. Phys. Chem. B* **2009**, *113*, 1127. Guidon, M.; Schiffmann, F.; Hutter, J.; VandeVondele, J. *J. Chem. Phys.* **2008**, *128*, 214104. Lee, H.-S.; Tuckerman, M. E. *J. Chem. Phys.* **2007**, *126*, 164501. Lee, H.-S.; Tuckerman, M. E. *J. Phys. Chem. A* **2006**, *110*, 5549. McGrath, M. J.; Siepmann, J. I.; Kuo, I. F. W.; Mundy, C. J.; VandeVondele, J.; Hutter, J. *J. Phys. Chem. A* **2005**, *110*, 640. Sit, P. H. L.; Marzari, N. *J. Chem. Phys.* **2005**, *122*, 204510. Schweigler, E.; Grossman, J. C.; Gygi, F.; Galli, G. *J. Chem. Phys.* **2004**, *121*, 5400. Fernandez-Serra, M. V.; Artacho, E. *J. Chem. Phys.* **2004**, *121*, 11136. Asthagiri, D.; Pratt, L. R.; Kress, J. D. *Phys. Rev. E* **2003**, *68*, No. 041505. Sprik, M.; Hutter, J.; Parrinello, M. *J. Chem. Phys.* **1996**, *105*, 1142. Kim, K.; Jordan, K. D. *J. Phys. Chem.* **1994**, *98*, 10089. Buch, V.; Milet, A.; Vacha, R.; Jungwirth, P.; Devlin, J. P. *Proc. Natl. Acad. Sci. U.S.A.* **2007**, *104*, 7342.

(20) Svozil, D.; Jungwirth, P. *J. Phys. Chem. A* **2006**, *110*, 9194.

(21) Kohn, W.; Sham, L. J. *Phys. Rev.* **1965**, *140*, A1133.

(22) Perdew, J. P.; Yue, W. *Phys. Rev. B* **1986**, *33*, 8800.

(23) Becke, A. D. *Phys. Rev. A* **1988**, *38*, 3098.

(24) Lee, C. T.; Yang, W. T.; Parr, R. G. *Phys. Rev. B* **1988**, *37*, 785.

(25) Becke, A. D. *J. Chem. Phys.* **1993**, *98*, 1372. Becke, A. D. *J. Chem. Phys.* **1993**, *98*, 5648.

(26) Sodupe, M.; Bertran, J.; Rodriguez-Santiago, L.; Baerends, E. J. *J. Phys. Chem. A* **1999**, *103*, 166.

(27) Lee, H. M.; Kim, K. S. *J. Chem. Theory Comput.* **2009**, *9*, 976.

(28) d'Avezac, M.; Calandra, M.; Mauri, F. *Phys. Rev. B* **2005**, *71*, 205210. VandeVondele, J.; Sprik, M. *Phys. Chem. Chem. Phys.* **2005**, *7*, 1363. Mantz, Y. A.; Gervasio, F. L.; Laino, T.; Parrinello, M. *J. Phys. Chem. A* **2006**, *111*, 105.

(29) Merkle, R.; Savin, A.; Preuss, H. *J. Chem. Phys.* **1992**, *97*, 9216.

(30) Bally, T.; Sastry, G. N. *J. Phys. Chem. A* **1997**, *101*, 7923.

(31) Lundberg, M.; Siegbahn, P. E. M. *J. Chem. Phys.* **2005**, *122*. Perdew, J. P.; Ruzsinszky, A.; Csonka, G. I.; Vydrov, O. A.; Scuseria, G. E.; Staroverov, V. N. *Phys. Rev. A* **2007**, *76*, No. 040501. Ruzsinszky, A.; Perdew, J. P.; Csonka, G. I.; Vydrov, O. A.; Scuseria, G. E. *J. Chem. Phys.* **2007**, *126*, 104102. Kaupp, M.; Bahmann, H.; Arbuznikov, A. V. *J. Chem. Phys.* **2007**, *127*, 194102.

(32) Livshits, E.; Baer, R. *J. Phys. Chem. A* **2008**, *112*, 12789.

(33) Seidl, A.; Gorling, A.; Vogl, P.; Majewski, J. A.; Levy, M. *Phys. Rev. B* **1996**, *53*, 3764.

(34) Savin, A. Beyond the Kohn-Sham Determinant. In *Recent Advances in Density Functional Methods Part I*; Chong, D. P., Ed.; World Scientific: Singapore, 1995; p 129.

(35) Iikura, H.; Tsuneda, T.; Yanai, T.; Hirao, K. *J. Chem. Phys.* **2001**, *115*, 3540. Yanai, T.; Tew, D. P.; Handy, N. C. *Chem. Phys. Lett.* **2004**, *393*, 51.

(36) Baer, R.; Neuhauser, D. *Phys. Rev. Lett.* **2005**, *94*, No. 043002.

(37) Livshits, E.; Baer, R. *Phys. Chem. Chem. Phys.* **2007**, *9*, 2932.

(38) Henderson, T. M.; Janesko, B. G.; Scuseria, G. E. *J. Phys. Chem. A* **2008**, *112*, 12530.

(39) Baer, R.; Livshits, E.; Salzner, U. *Annu. Rev. Phys. Chem.* **2010**, *61*, 85.

(40) Leininger, T.; Stoll, H.; Werner, H.-J.; Savin, A. *Chem. Phys. Lett.* **1997**, *275*, 151.

(41) Perdew, J. P.; Parr, R. G.; Levy, M.; Balduz, J. L. *Phys. Rev. Lett.* **1982**, *49*, 1691.

(42) Cohen, A. J.; Mori-Sanchez, P.; Yang, W. T. *Phys. Rev. B* **2008**, *77*, 115123.

(43) Peach, M. J. G.; Helgaker, T.; Salek, P.; Keal, T. W.; Lutnaes, O. B.; Tozer, D. J. *Phys. Chem. Chem. Phys.* **2006**, *8*, 558. Chai, J. D.; Head-Gordon, M. *J. Chem. Phys.* **2008**, *128*, No. 084106. Vydrov, O. A.; Scuseria, G. E. *J. Chem. Phys.* **2006**, *125*, 234109. Gerber, I. C.; Angyan, J. G. *Chem. Phys. Lett.* **2005**, *415*, 100. Cohen, A. J.; Mori-Sanchez, P.; Yang, W. T. *J. Chem. Phys.* **2007**, *126*, 191109.

(44) Almbladh, C.-O.; von-Barth, U. *Phys. Rev. B* **1985**, *31*, 3231.

(45) Stein, T.; Kronik, L.; Baer, R. *J. Am. Chem. Soc.* **2009**, *131*, 2818. Stein, T.; Kronik, L.; Baer, R. *J. Chem. Phys.* **2009**, *131*, 244119.

- (46) Salzner, U.; Baer, R. *J. Chem. Phys.* **2009**, *131*, 231101.
- (47) Banna, M. S.; McQuaide, B. H.; Malutzki, R.; Schmidt, V. *J. Chem. Phys.* **1986**, *84*, 4739.
- (48) Reutt, J. E.; Wang, L. S.; Lee, Y. T.; Shirley, D. A. *J. Chem. Phys.* **1986**, *85*, 6928.
- (49) Tomoda, S.; Achiba, Y.; Kimura, K. *Chem. Phys. Lett.* **1982**, *87*, 197.
- (50) Foner, S. N.; Hudson, R. L. *J. Chem. Phys.* **1956**, *25*, 602.
- (51) Winter, B.; Faubel, M.; Hertel, I. V.; Pettenkofer, C.; Bradforth, S. E.; Jagoda-Cwiklik, B. *J. Am. Chem. Soc.* **2006**, *128*, 3864.
- (52) Shao, Y.; Molnar, L. F.; Jung, Y.; Kussmann, J.; Ochsenfeld, C.; Brown, S. T. *Phys. Chem. Chem. Phys.* **2006**, *8*, 3172.
- (53) Baroni, S.; Dal Corso, A.; S., d. G.; Giannozzi, P.; Cavazzoni, C.; Ballabio, G.; et al. <http://www.pwscf.org/>.
- (54) Eisenberg, H. R.; Baer, R. *Phys. Chem. Chem. Phys.* **2009**, *11*, 4674.
- (55) Bylaska, E. J.; de Jong, W. A.; Govind, N.; Kowalski, K.; Straatsma, T. P.; Valiev, M. et al. *Wchem A Computational Chemistry Package for Parallel Computers, Version 5.1*; Pacific Northwest National Laboratory, Richland, WA, 2007.
- (56) Sodupe, M.; Bertran, J.; Rodriguez-Santiago, L.; Baerends, E. J. *J. Phys. Chem. A* **1998**, *103*, 166.
- (57) Potts, A. W.; Price, W. C. *Proc. R. Soc. London, Ser. A* **1972**, *326*, 181.
- (58) Sodupe, M.; Oliva, A.; Bertran, J. *J. Am. Chem. Soc.* **1994**, *116*, 8249. Gill, P. M. W.; Radom, L. *J. Am. Chem. Soc.* **1988**, *110*, 4931.
- (59) Granot, R.; Baer, R. *J. Chem. Phys.* **2008**, *128*, 184111.
- (60) Andersen, H. C. *J. Chem. Phys.* **1980**, *72*, 2384.
- (61) Guillot, B. *J. Chem. Phys.* **1991**, *95*, 1543.
- (62) Douberly, G. E.; Walters, R. S.; Cui, J.; Jordan, K. D.; Duncan, M. A. *J. Phys. Chem. A* **2010**, *114*, 4570.
- (63) Wei, M.; He, C.; Hua, W.; Duan, C.; Li, S.; Meng, Q. *J. Am. Chem. Soc.* **2006**, *128*, 13318.
- (64) Stein, T.; Baer, R.; Kronik, L. Work in progress, 2010. Livshits, E.; Baer, R.; Kosloff, R. *J. Phys. Chem. A* **2009**, *113*, 7521. Andzelm, J.; Rinderspacher, B. C.; Rawlett, A.; Dougherty, J.; Baer, R.; Govind, N. *J. Chem. Theory Comput.* **2009**, *5*, 2835. Baer, R.; Livshits, E.; Neuhauser, D. *Chem. Phys.* **2006**, *329*, 266.
- (65) Cohen, A. J.; Mori-Sanchez, P.; Yang, W. T. *Science* **2008**, *321*, 792.